Draft version October 22, 2008
Preprint typeset using LaTeX style emulateapj v. 10/09/06

THE PROMPT, HIGH RESOLUTION SPECTROSCOPIC VIEW OF THE "NAKED-EYE" GRB080319B *

V. D'Elia[1], F. Fiore[1], R. Perna[2], Y. Krongold[3], S. Covino[4], D. Fugazza[4], D. Lazzati[2], F. Nicastro[1], L.A. Antonelli[1], S. Campana[4], G. Chincarini[4,5], P. D'Avanzo[4], M. Della Valle[6], P. Goldoni[7], D. Guetta[1], C. Guidorzi[4], E.J.A. Meurs[8,9], F. Mirabel[10], E. Molinari[4], L. Norci[9], S. Piranomonte[1], L. Stella[1], G. Stratta[11], G. Tagliaferri[4], P. Ward[8,12].

Draft version October 22, 2008

ABSTRACT

GRB080319B reached 5th optical magnitude during the burst prompt emission. Thanks to the VLT/UVES rapid response mode, we observed its afterglow just 8m:30s after the GRB onset when the magnitude was R $\sim$ 12. This allowed us to obtain the best signal-to-noise, high resolution spectrum of a GRB afterglow ever (S/N per resolution element $\sim$ 50). The spectrum is rich of absorption features belonging to the main system at z=0.937, divided in at least six components spanning a total velocity range of 100 km s^{-1}. The VLT/UVES observations caught the absorbing gas in a highly excited state, producing the strongest Fe II fine structure lines ever observed in a GRB. A few hours later the optical depth of these lines was reduced by a factor of 4-20, and the optical/UV flux by a factor of $\sim$ 60. This proves that the excitation of the observed fine structure lines is due to "pumping" by the GRB UV photons. A comparison of the observed ratio between the number of photons absorbed by the excited state and those in the Fe II ground state suggests that the six absorbers are $\sim 2-6$ kpc from the GRB site, with component I $\sim$ 3 times closer to the GRB site than components III to VI. Component I is characterized also by the lack of Mg I absorption, unlike all other components. This may be due both to a closer distance and a lower density, suggesting a structured ISM in this galaxy complex.

Subject headings: Gamma Ray Bursts

1. INTRODUCTION

For a few hours after their onset, Gamma Ray Burst (GRB) afterglows are the brightest beacons in the far Universe. In a small fraction of the cases, extremely bright optical transient emission is associated with the GRB event, offering a superb opportunity to investigate high–z galaxies through high resolution spectroscopy of the optical transient. The study of the rich absorption spectra can yield unique information on the gas in the GRB environment and the physical, chemical and dynamical state and geometry of the inter–stellar matter (ISM) of intervening galaxies, including the GRB host galaxy.

GRB080319B was discovered by the Burst Alert Telescope (BAT) instrument on board Swift on 2008, March 19, at 06:12:49 UT. Swift slewed to the target in less than 1 minute and a bright afterglow was found by both the X-Ray Telescope (XRT) and UV-Optical Telescope (UVOT) at RA = 14h 31m 40.7s, Dec = $+36^o$ 18′ 14.7" (Racusin et al. 2008a) with observations starting 60.5 and 175 s after the trigger, respectively. The field of GRB080319B was imaged by the "Pi of the Sky" apparatus located at Las Campanas Observatory before, during and after the GRB event (Cwiok et al. 2008). The field was also targetted by the robotic telescope REM just 43 s after the BAT trigger (Covino et al. 2008a, b). The TORTORA wide-field optical camera (12 cm diameter, 20×25 deg FOV, TV-CCD, unfiltered) mounted on REM also imaged the field before, during and after the GRB event with good temporal resolution (Karpov et al. 2008). These observations show that the GRB reached the magnitudes $V = 5.3$ about 20 s and $H = 4.2$ about 50 s after the trigger. This makes GRB080319B the brightest GRB ever recorded at optical wavelengths (Bloom et al. 2008, Racusin et al. 2008b).

The optical afterglow of GRB080319B was observed at high resolution with VLT/UVES starting just 8m:30s after the BAT trigger, thanks to the VLT rapid response mode (RRM), when its magnitude was R$\sim 12 \div 13$. This allowed us to obtain the best signal-to-noise, high resolution spectrum of a GRB afterglow ever (S/N per resolution element $\sim$ 50). Two further RRM and target of opportunity (ToO) observations were obtained $2-3$

*BASED ON OBSERVATIONS COLLECTED AT THE EUROPEAN SOUTHERN OBSERVATORY (ESO) WITH THE VLT/KUEYEN TELESCOPE, PARANAL, CHILE, IN THE FRAMEWORK OF PROGRAM 080.A-0398.

Electronic address: delia@oa-roma.inaf.it
[1] INAF, Osservatorio Astronomico di Roma, via Frascati 33, Monteporzio (Rm), I00040, Italy;
[2] JILA and Department of Astrophysical and Planetary Science, CU Boulder, Boulder, 80309, USA;
[3] Instituto de Astronomia, Universidad Nacional Autonomica de Mexico, Apartado Postal 70-264, 04510 Mexico DF;
[4] INAF, Osservatorio Astronomico di Brera, via E. Bianchi 46, 23807 Merate (LC), Italy;
[5] Universita' di Milano Bicocca, piazza della Scienza 3, 20126 Milano, Italy
[6] INAF, Osservatorio Astronomico di Capodimonte, salita Moiarello 16, Napoli, Italy;
[7] APC/UMR 7164, Service dAstrophysique, CEA Centre de Saclay;
[8] School of Cosmic Physics, DIAS, 31 Fitzwilliam Place, Dublin 4, Ireland;
[9] School of Physical Sciences and NCPST, DCU, Glasnevin, Dublin 9, Ireland;
[10] European Southern Observatory, Casilla 19001, Santiago, Chile;
[11] ASI Science Data Center, via Galileo Galilei, 00044 Frascati, Italy
[12] Mullard Space Science Laboratory, Dorking, Surrey RH5 6NT, UK.

TABLE 1
GRB080319B journal of observations

Obs	UT observation	T. from burst (s)	Exp. (s)	S/N range	Dichroics	Arms	R mag
RRM 1	2008 Mar 19, 06:21:26	517	600	$30 \div 50$	2	Blue + Red	$12 \div 13$
RRM 2	2008 Mar 19, 08:06:42	6833	1800	$7 \div 12$	$1 + 2$	Blue + Red	$16 \div 17$
ToO	2008 Mar 19, 09:07:22	10482	1200	$5 \div 8$	$1 + 2$	Blue + Red	$16 \div 17$

hours after the event. Several absorption systems are present in these spectra. Vreeswijk et al. (2008) identify the highest redshift system at 0.937 as the GRB host galaxy.

This paper concentrates on the analysis of the Fe II excited lines associated with the main system at z=0.937 and on their variability. Section 2 describes the datasets and data analysis; Section 3 presents the UVES spectroscopy and discusses the absorption features and their variability; Section 4 concerns the evaluation of the distance of the absorbers from the GRB explosion site; our conclusions are given in Section 5. A $H_0 = 70$ km s^{-1} Mpc^{-1}, Ω_M=0.3, $\Omega_\Lambda = 0.7$ cosmology is adopted throughout.

2. OBSERVATIONS AND DATA ANALYSIS

We observed the bright afterglow of GRB080319B in the framework of the ESO program 080.A-0398 with the VLT/UVES (Dekker et al. 2000). The Observation Log is reported in Table 1. Both UVES dichroics, as well as the red and the blue arms, were used.

The first, 10min observation, was performed in RRM and started just 8m:30s after the GRB event, when the afterglow was extremely bright (R=12-13). This afforded a S/N=$30 \div 50$ per resolution element. Two more UVES observations followed, the first one again in RRM mode, activated in the framework of program 080.D-0526 and starting 1.9 hours after the GRB event, and the second a ToO, starting 2.9 hours after the GRB, see Table 1.

Data reduction was carried out by using the UVES pipeline (Ballester et al. 2000). The final useful spectra extend from $\sim$ 3800 Å to $\sim$ 9500 Å. The resolution element, set to two pixels, ranges then from 4 km s^{-1} at 4500 Å to 1.9 km s^{-1} at 9000 Å. The noise spectrum, used to determine the errors on the best fit line parameters, was calculated from the real-background-subtracted spectra using line-free regions. This takes into account both statistical and systematic errors in the pipeline processing and background subtraction.

3. UVES SPECTROSCOPY OF EXCITED LINES

The three UVES observations were analyzed in the MIDAS environment using the FITLYMAN procedure (Fontana & Ballester 1995). The highest z system present in these spectra is at z=0.937, as also reported by Vreeswijk et al. (2008). This system presents absorption features from the ground states of MgI, MgII, FeII and several FeII fine structure lines (FeII* hereafter). The most striking feature in the UVES spectra is the variation of the opacity of the fine structure lines between the first and the second UVES observation. Fig. 1 shows the Fe IIλ2374 and Fe II$^*\lambda$2396 absorption features in the three epochs. We see strong variations of both lines. While the strength of the Fe IIλ2374 absorption increases from the first to the third epoch, strong Fe II$^*\lambda$2396 absorption is present only in the first spectrum and nearly disappears in the second and third spectra. The huge variations of Fe II fine structure lines imply that "pumping" by the GRB UV photons is the main mechanism for populating the excited states (Silva & Viegas 2002; Prochaska et al. 2006; Vreeswijk et al. 2007).

UVES spectra of bright GRB afterglows have always revealed a complex structure of the absorption system associated with the GRB host galaxy, reflecting the clumpy nature of the ISM (see e.g. D'Elia et al. 2007). This is confirmed by the UVES spectra of GRB080319B. A detailed line fitting was performed using a Voigt profile with three parameters: the line wavelength, column density and Doppler parameter b. Several absorption features were fitted simultaneously by keeping the redshift and b value of each component fixed at their common values (best fit b values in the $3 \div 10$ range). The Fe II$^*\lambda$2396 absorption lines are not saturated, and can be used to guide the identification of different components. Statistically acceptable fits to the first epoch UVES spectrum are obtained by using six components. These span a range of $\sim$ 100 km s^{-1} in velocity space. Fig. 2 shows the best fitting model to the Mg Iλ2026, Fe IIλ2382 and Fe II$^*\lambda$2396 lines. The lower S/N spectra from the second and third epochs were then fitted by fixing the z and b parameters of each component at their respective best fit values found for the first epoch, highest S/N spectrum.

Table 2 gives the Mg I and Fe II and column densities of each of the six components in the three epochs. Components are labeled from I to VI for decreasing wavelengths (and decreasing redshift, or positive velocity shift with respect to a zero point, placed at z=0.9371). Fe II is represented by the ground, first excited ($4F$) and second excited (^4D) levels. Fine structures of each level are marked with asterisks; the ground state shows four fine structure levels, the excited ones just the first level. The second column indicates which transitions have been used to evaluate the column density of each ionic specie. Strong Mg II absorption is present for all components, but reliable column densities cannot be derived for this ion because the lines are strongly saturated. The column density uncertainties are given at the 1σ confidence level, while upper limits are at a 90% confidence level (i.e. 1.6σ). The column densities derived from the second epoch spectrum are always consistent with those derived from the third epoch spectrum, to within their relatively large errors. Thus, in order to improve the S/N, we also added together the second and third epoch spectra and repeated the fits.

Mg I is detected for all components but I. The Mg I column density of the five detected components is consistent with a constant value (within each component) at all epochs. Conversely, we see strong variations in time of both Fe II excited and ground state lines for all six components. The Fe II fine structures line of the lower redshift components underwent the strongest variations, as most of these lines are not detected in the second and

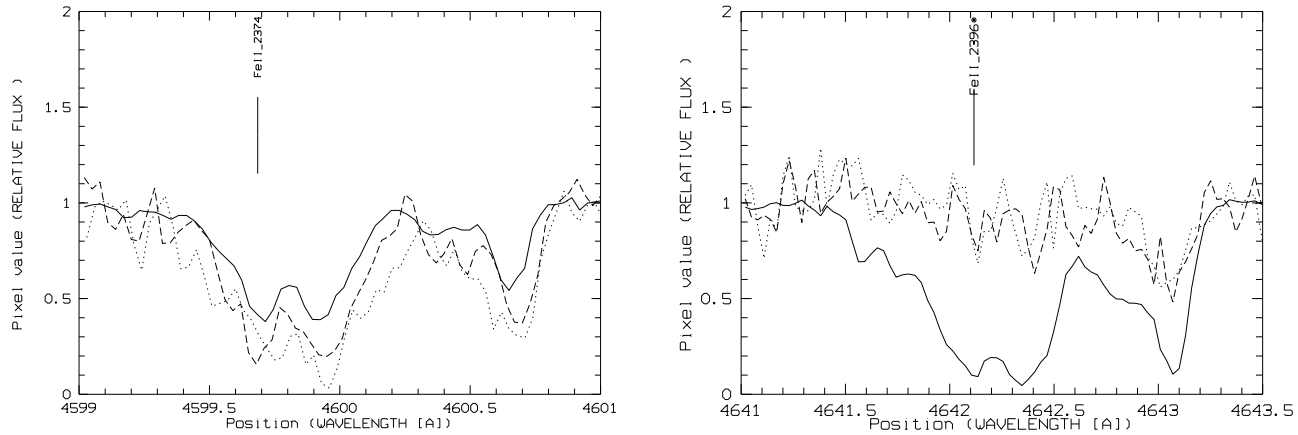

FIG. 1.— The UVES spectra of GRB080319B around the Fe IIλ2374 (left panel) and Fe IIλ2396* (right panel) transitions. Solid lines refer to the first epoch spectrum (8m30s after the Swift trigger), dashed lines to the second epoch spectrum (1.9 hours after the GRB event), and dotted lines to the the third epoch spectrum (2.9 hours after the GRB event).

third epoch spectra. The Fe II first fine structure line of the highest redshift component I varies less, and it is still detected in the second and third epoch spectra. Fig. 3 compares the column density of the Fe II$^*\lambda$2396 line of the six components in the first epoch spectrum to that measured 2-3 hr later. The column density of component I dropped by a factor of ~ 4, while that of component III dropped by a factor of ~ 20 (Table 3). On the other hand, the column density of ground state Fe II increased by a factor of 1.3-2 for all six components (Table 3). The de-excitation of the excited levels into ground state levels, as time passes and the UV radiation field diminishes, is certainly contributing to this increase. For all components, the increase in the column density of the Fe II resonant line is consistent with the decrease of the excited lines within 1σ. This is a first indication that the absorbing medium must be relatively distant, since photoionization of the medium by the burst photons, predicted to be important in the vicinity of the source (Perna & Loeb 1998; Perna & Lazzati 2002) appears to be negligible here.

4. DISTANCE OF THE ABSORBERS FROM THE GRB

A constraint on the distance of the absorbing gas to the GRB can be obtained using the ratio between the number of photons absorbed by the first fine structure level of Fe II and its corresponding ground state. This ratio in the prompt spectrum of GRB080319B is 0.6 for component I and II, between 0.3 and 0.4 for components III, IV, V and VI. Note that the value for component I and II is close to the maximum theoretical value of 0.8. As a comparison, the same ratio in the prompt spectrum of GRB060418 was 0.09 (Vreeswijk et al. 2007). Calculations of population ratios (Silva & Viegas 2002; see also Prochaska, Chen & Bloom 2006) show that the observed ratios are obtained for a UV flux of $\sim 3\times10^6-10^7\ G_0$ for the six components, where $G_0 = 1.6\times10^{-3}$ erg cm^{-2} s^{-1}. This implies distances from the GRB to the six absorbers $R = \left[L_{UV}/(4\pi G_0 \times (3\times10^6 - 10^7))\right]^{1/2} \approx 18-34$ kpc (having assumed $L_{UV} = 6.7\times10^{50}$ erg s^{-1}, obtained integrating the light curve by Racusin et al. 2008b).

However, these population ratios are calculated assuming a steady-state ionizing flux, an approximation which is not an appropriate description for a GRB afterglow.

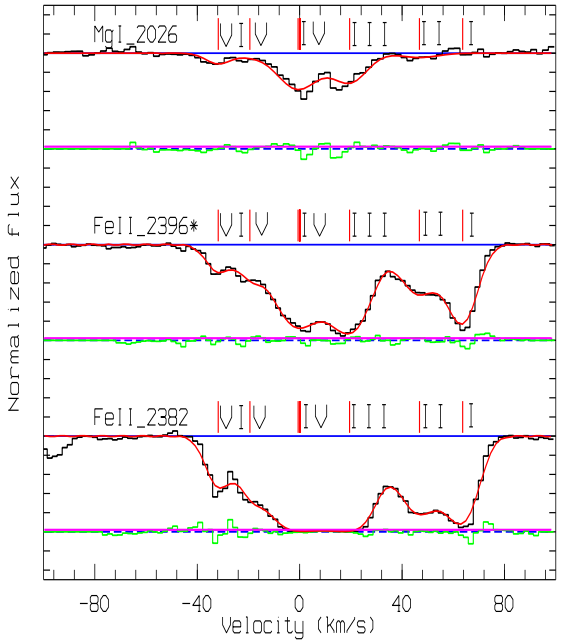

FIG. 2.— The first UVES spectrum of GRB080319B around the MgIλ2026, FeIIλ2396* and FeIIλ2382 transitions. The solid line shows the six component fit (I to VI from higher to lower redshift). The velocity position of the components is marked with vertical lines, as well as the zero point at $z = 0.9371$.

To obtain a more reliable result, we built up a time dependent photoexcitation code to compute the column densities of the excited states as a function of the absorbing gas distance from the GRB, in a similar way to that of Vreeswijk et al. (2007). The basic equation to be solved is the balance equation:

$$\frac{dN_u}{dt} = N_l B_{lu} F_\nu(\tau_0) - N_u[A_{ul} + B_{ul} F_\nu(\tau_0)], \quad (1)$$

which describes the transition between two atomic levels. It gives the increment in the upper level population N_u as a function of the lower level N_l, the flux $F_\nu(\tau_0)$ experienced by the absorber, and the Einstein coefficients A and B. In more detail, A_{ul} represents the sponta-

TABLE 2
MgI, FeII and FeII* column densities for the six components at three epochs.

Specie	Trans.	Obs.	I (64 km/s)	II (47 km/s)	III (20 km/s)	IV (0 km/s)	V (-20 km/s)	VI (-32 km/s)
Mg I	λ2026	1	< 11.80	12.14 ± 0.10	13.00 ± 0.02	13.18 ± 0.01	11.83 ± 0.17	12.38 ± 0.05
	λ2852	2	< 11.2	12.09 ± 0.03	13.06 ± 0.08	12.94 ± 0.12	11.77 ± 0.06	12.02 ± 0.05
		3	< 11.6	12.05 ± 0.04	13.39 ± 0.11	12.87 ± 0.10	11.81 ± 0.07	12.05 ± 0.07
		2+3	< 11.0	12.08 ± 0.02	13.18 ± 0.06	12.95 ± 0.07	11.80 ± 0.05	12.07 ± 0.05
FeII	λ2374	1	13.52 ± 0.01	13.11 ± 0.02	13.84 ± 0.02	13.79 ± 0.02	12.76 ± 0.02	12.77 ± 0.02
	λ2382	2	13.78 ± 0.05	13.26 ± 0.09	14.13 ± 0.05	14.01 ± 0.06	13.11 ± 0.06	12.86 ± 0.22
		3	13.99 ± 0.07	13.19 ± 0.17	14.32 ± 0.10	13.99 ± 0.11	12.77 ± 0.85	12.81 ± 0.34
		2+3	13.87 ± 0.04	13.24 ± 0.10	14.19 ± 0.08	14.00 ± 0.10	13.00 ± 0.12	12.84 ± 0.17
FeII*	λ2333	1	13.29 ± 0.02	12.90 ± 0.02	13.37 ± 0.02	13.36 ± 0.02	12.40 ± 0.06	12.30 ± 0.05
	λ2365	2	12.66 ± 0.05	12.33 ± 0.04	< 12.2	< 12.2	< 12.2	< 12.2
	λ2389	3	12.66 ± 0.11	< 12.6	< 12.6	< 12.6	< 12.6	< 12.6
	λ2396	2+3	12.67 ± 0.11	12.15 ± 0.12	12.13 ± 0.12	< 12.0	< 12.0	< 12.0
FeII**	λ2328	1	13.03 ± 0.01	12.53 ± 0.01	13.20 ± 0.01	13.16 ± 0.01	12.45 ± 0.01	11.78 ± 0.27
		2	< 13.0	< 13.0	< 13.0	< 13.0	< 13.0	< 13.0
		3	< 13.4	< 13.4	< 13.4	< 13.4	< 13.4	< 13.4
		2+3	< 12.8	< 12.8	< 12.8	< 12.8	< 12.8	< 12.8
FeII***	λ2338	1	12.86 ± 0.02	12.48 ± 0.04	13.02 ± 0.02	13.02 ± 0.02	11.89 ± 0.13	11.82 ± 0.13
	λ2359	2	< 13.0	< 13.0	< 13.0	< 13.0	< 13.0	< 13.0
		3	< 13.4	< 13.4	< 13.4	< 13.4	< 13.4	< 13.4
		2+3	< 12.8	< 12.8	< 12.8	< 12.8	< 12.8	< 12.8
FeII****	λ2345	1	12.54 ± 0.02	12.24 ± 0.04	12.79 ± 0.02	12.76 ± 0.02	11.78 ± 0.37	11.70 ± 0.10
	λ2414	2	< 12.7	< 12.7	< 12.7	< 12.7	< 12.7	< 12.7
		3	< 13.1	< 13.1	< 13.1	< 13.1	< 13.1	< 13.1
		2+3	< 12.5	< 12.5	< 12.5	< 12.5	< 12.5	< 12.5
FeII ^{4}F	λ2332	1	13.25 ± 0.02	12.18 ± 0.24	13.62 ± 0.01	13.42 ± 0.02	12.37 ± 0.12	12.12 ± 0.23
	λ2360	2	< 12.7	< 12.7	< 12.7	< 12.7	< 12.7	< 12.7
		3	< 13.1	< 13.1	< 13.1	< 13.1	< 13.1	< 13.1
		2+3	13.21 ± 0.09	12.6 ± 0.36	13.59 ± 0.07	13.35 ± 0.09	< 12.5	12.37 ± 0.52
FeII ^4F*	λ2361	1	12.73 ± 0.04	< 11.5	12.95 ± 0.04	12.74 ± 0.05	12.69 ± 0.09	12.25 ± 0.16
		2	< 12.7	< 12.7	< 12.7	< 12.7	< 12.7	< 12.7
		3	< 13.1	< 13.1	< 13.1	< 13.1	< 13.1	< 13.1
		2+3	< 12.5	< 12.5	< 12.5	< 12.5	< 12.5	< 12.5
FeII ^4D	λ2563	1	12.60 ± 0.02	11.72 ± 0.16	11.99 ± 0.10	11.80 ± 0.15	< 11.5	< 11.5
		2	< 12.7	< 12.7	< 12.7	< 12.7	< 12.7	< 12.7
		3	< 13.1	< 13.1	< 13.1	< 13.1	< 13.1	< 13.1
		2+3	< 12.5	< 12.5	< 12.5	< 12.5	< 12.5	< 12.5
FeII ^4D*	λ2564	1	12.37 ± 0.05	< 11.5	11.97 ± 0.13	11.53 ± 0.36	< 11.5	< 11.5
		2	< 12.7	< 12.7	< 12.7	< 12.7	< 12.7	< 12.7
		3	< 13.1	< 13.1	< 13.1	< 13.1	< 13.1	< 13.1
		2+3	< 12.5	< 12.5	< 12.5	< 12.5	< 12.5	< 12.5

All values are logarithmic cm^{-2}

TABLE 3
The Fe II and Fe II* column density ratios between observation 1 and 2+3.

	I	II	III	IV	V	VI
Fe II	-0.35 ± 0.05	-0.13 ± 0.12	-0.35 ± 0.10	-0.21 ± 0.12	-0.24 ± 0.14	-0.07 ± 0.19
Fe II*	0.62 ± 0.13	0.75 ± 0.14	1.24 ± 0.14	> 1.36	> 0.40	> 0.30

Ratios are expressed in logarithmic cm^{-2}

neous decay from the upper to the lower state, $B_{ul} = A_{ul}\lambda^3/2hc$ the stimulated emission, and $B_{lu} = B_{ul}g_u/g_l$ the absorption. Here λ is the transition wavelength and g the degeneracy of the levels. $F_\nu(\tau_0)$ is the monochromatic flux at the transition frequency:

$$F_\nu(\tau_0) = F_\nu(0)e^{-\tau} + S_\nu(1 - e^{-\tau}), \quad (2)$$

corrected by the optical depth at the line center $\tau_0 = 1.497\ 10^{-2} N_l \lambda f / b$ (cgs units); b is the Doppler factor of the transition and f its oscillator strength, which is related to the Einstein coefficient A by:

$$f = \frac{m_e c A_{ul} g_u \lambda^2}{8\pi^2 q_e^2 g_l}. \quad (3)$$

The source function of the radiative transfer equation (2) is defined as:

$$S_\nu = \frac{N_u(\nu) A_{ul}}{N_l(\nu) B_{lu} - N_u(\nu) B_{ul}} \quad (4)$$

(Lequeux 2005). Finally, the uncorrected flux experienced by the absorber is:

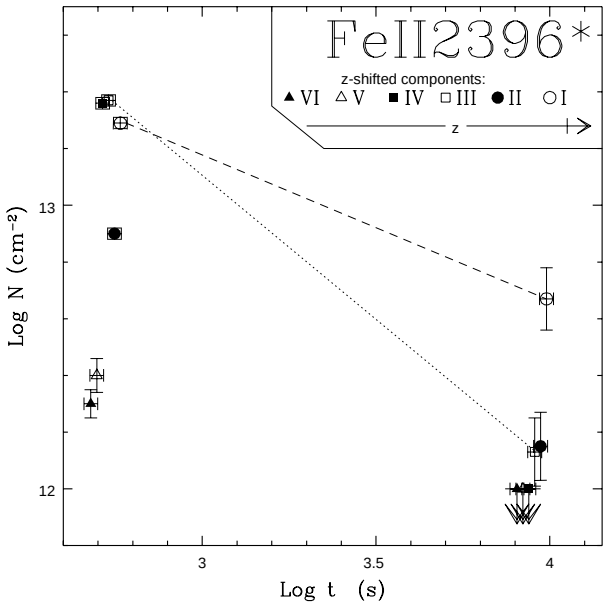

FIG. 3.— The column density of the FeIIλ2396* line for the six components as a function of time. For clarity reasons, components have been slightly shifted with each other. Late time points represent the observations 2 and 3 added together. Note that the highest redshift component I varies less than the lower redshift components III and IV (the dashed and dotted lines are for components I and III, respectively).

$$F_\nu(0) = \frac{F_{br}\ (t/t_{br})^{-\alpha_{br}} (\lambda/5439\text{Å})^{-\beta_{br}} (d_{L,GRB}/d)^2}{1+z}, \quad (5)$$

(in cgs units) with z the GRB redshift used to compute its luminosity distance $d_{L,GRB}$ and d the distance of the absorber from the GRB. The normalization constant F_{br} and the temporal and spectral indices, α_{br} and β_{br}, have been taken from the paper by Racusin et al. (2008b). The optical light curve of GRB080319B in the V band (5439 Å) is not monotonic, but can be described by a broken power law with at least four different slopes in the time interval between 20 and 10^4 s from the GRB. For each break time t_{br}, we took the corresponding normalization constant F_{br} and the temporal and spectral indices, α_{br} and β_{br}, given in Racusin et al. (2008b).

Eq.1 must be simultaneously solved for many transitions, connecting in principle all the levels of a given atom or ion (Fe II in our case). We included in our computation a total of 38 levels, the 16 lowest levels plus 22 higher excited states. The atomic data for the transitions among these levels have been taken from Quinet et al. (1996) (for transitions between the low energy states) and the NIST database for other transitions (at the website http://physics.nist.gov/PhysRefData/ASD/index.html). In order to verify that the number of included transitions was large enough, we ran our code with the input parameters used by Vreeswijk et al. (2007) for GRB060418, and we found column densities fully consistent with their results.

We stress that collisional processes and/or direct infrared pumping (IR) alone can not be responsible for the variability we observe. If the first mechanism is at work, i.e. if the variability is produced by a decreasing temperature, we should observe a reduction of all the column densities of the excited states. Table 2 shows that fine structure levels dramatically decrease, but the first excited level (Fe II ^{4}F) stays almost constant in all components. On the other hand, in case of pure IR pumping (assuming that the dominant UV pumping process is for some reason inhibited), the fine structure levels of the ground state should be more populated than those for higher excited levels, which again is not observed. For more details on the competition between such mechanisms, see again Vreeswijk et al. (2007).

We ran our code using the total Fe II column densities and Doppler factors observed for components I and III ($N = 1.16\ 10^{14}$ and $1.88\ 10^{14}$ cm^{-2}, $b = 5$ and 10 km s^{-1}, respectively). The distance from the absorber was set as a free parameter in order to obtain the best agreement between the data and the photoexcitation code. In Fig.4 we show the results from our code. Dotted, solid and dashed lines represent the predictions for ground, fine structure and other excited levels, respectively. Short (long) dashed lines are for Fe II ^{4}F and ^{4}F* (^{4}D and ^{4}D*) levels. The data are reported as follows. Open circles represent the ground state levels, closed circle the fine structures of the ground state of Fe II, open squares Fe II ^{4}F and ^{4}F* and open triangles Fe II ^{4}D and ^{4}D*. The data represent the first and second+third observation, and have been slightly shifted to each other for clarity reasons. Fig. 4 shows that the time evolution of the Fe II column densities of component I is best reproduced by a model with an absorber located at 2 kpc from the GRB (lefthand plot), while the behaviour of component III is well fitted with an absorber at 6 kpc from the GRB (righthand plot). The closer the gas to the GRB, the longer the excited levels tend to be populated with respect to the ground state. The "anomalous" behaviour of the Fe II ^{4}F level is due to its high spontaneous decay rate toward the ground state, which is ~ 3 hours.

In order for our results to be self-consistent, we need to make sure that, at the smallest distance of 2 kpc as derived for component I, Fe II is not photoionized away by the strong UV radiation of the burst. To this purpose, we performed a series of runs of the photoionization code by Perna & Lazzati (2002), which accounts for the radiative-transfer of the radiation. We first simulated a medium in thermal equilibrium at a temperature of $\sim 10^4$ K, and let the radiation from the burst, modeled as in eq.(5), propagate through it. For a range of densities between 10^{-3} and 10^3 cm^{-3}, we followed the concentration of Fe II and Mg I absorbers at a distance of 2kpc, while the radiation from the burst impinges on them. For densities $\sim 10^3$ cm^{-3}, the burst appears not to alter the initial concentration of Fe II and Mg I. As the density decreases down to about 10^{-2} cm^{-3}, the concentration of Fe II still remains unaltered, but Mg I begins to be photoionized significantly. This different behaviour is due to the fact that Fe II is screened by Hydrogen, because its photoionization threshold is just above that of H. For even lower densities, Fe II begins to get photoionized away. For a density of 10^{-3} cm^{-3}, the concentration of Fe II decreases by about 15% during the burst. These calculations show that there is a wide range of medium densities for which an Fe II absorber at a distance of 2 kpc is not photoionized away by the radiation from the

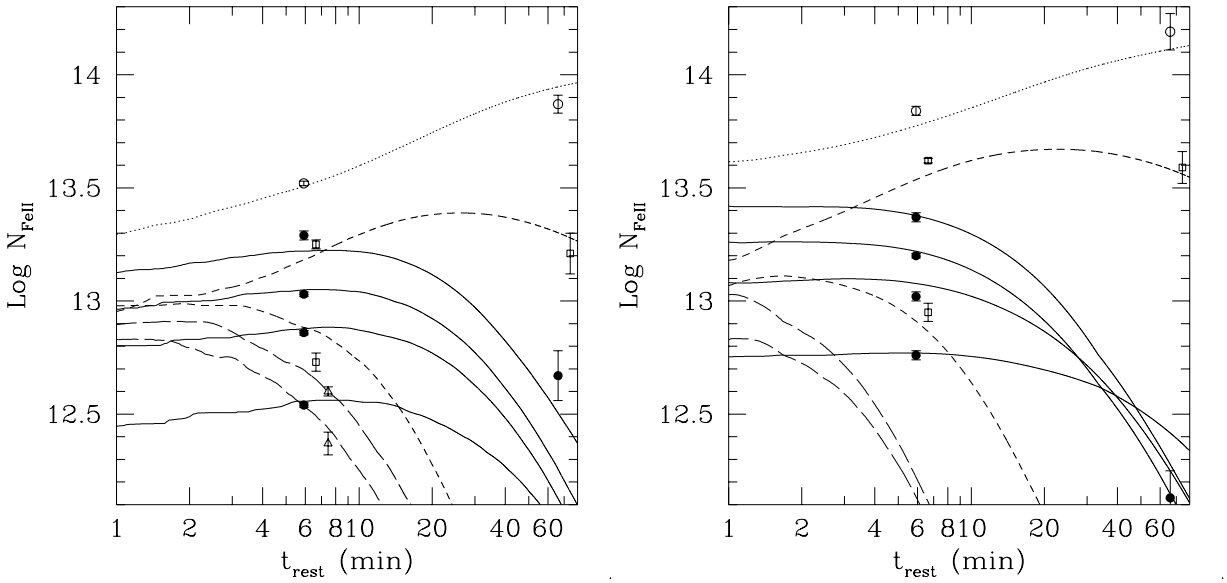

FIG. 4.— Time evolution of Fe II column densities for ground level (open circles), fine structure level (solid circles) and first (square) and second (triangles) excited level transitions for component I (lefthand plot) and III (righthand plot) in the spectrum of GRB080319b. Column density predictions from our time-dependent photo-excitation code are also shown. They refer to the ground level (dotted lines), fine structure levels (solid lines) and excited levels (dashed lines) transitions, in the case of an absorber at 2 kpc (lefthand plot) and at 6 kpc (righthand plot) from the GRB. For clarity reasons, data points have been slightly shifted to each others.

burst, while, on the other hand, Mg I is substantially destroyed. Interestingly, component I is the only one for which Mg I is below the detection limit.

5. DISCUSSION AND CONCLUSIONS

Thanks to the VLT RRM, which allowed the observation of GRB080319B in just 5min (rest frame), we were able to catch the absorbing gas in a highly excited state, producing the strongest Fe II fine structure lines ever observed in a GRB (or QSO) spectrum. The optical depth of these lines was dramatically reduced 2-3 hours later, implying a factor of 4-20 decrease for all six components belonging to the main absorption system. At the same time, the optical/UV flux dropped by a factor of ~ 60 (Bloom et al. 2008, Racusin et al. 2008b). The variation of the Fe II fine structure lines is spectacular, when compared to previous GRB observations. Before GRB080319B, the best case was certainly that of GRB060418 at z=1.490, observed with UVES on comparably short timescales. Vreeswijk et al. (2007) report for this burst variations of the Fe II fine structure lines column densities by a factor of 1.4, in spectra taken 700 s and 7680 s after the GRB onset; in the same time interval the optical/UV flux dropped by a factor of ~ 20. The variations seen in GRB080319B at similar rest frame timescales are clearly much more prominent. This is probably due to the extremely intense optical/UV radiation field of GRB080319B.

The optical GRB magnitude reached V$\sim$ 5.3 about 40 s after the start of the GRB event. At z=0.937, this magnitude implies a ~ 912Å ionizing luminosity L= 1.2×10^{51} erg s^{-1}, assuming a power law spectrum with frequency spectral index -1 and integrating it up to 1 keV. Since the Fe II ionization potential is just above the photoionization edge of H, this ion is efficiently screened and it can be photoionized only after H has been photoionized. We can compute the number of ionizing photons by integrating the optical/UV light curve (Bloom et al. 2008, Racusin et al. 2008b). We find $N_\gamma = 8.6 \times 10^{62}$ ph at 912Å; similar numbers are obtained by extrapolating the XRT X-ray spectrum down to 912Å assuming no absorption, in addition to the Galactic value along the line of sight.

We can constrain the distance of the absorbing gas to the GRB using these numbers and the ratio between the number of photons absorbed by the first fine structure level and the Fe II ground state. In a steady state approximation (Silva & Viegas 2002; see also Prochaska, Chen & Bloom 2006), this distance turns out to be ~ 18 and ~ 34 kpc for component I and III, respectively. Since GRBs are highly variable events, to refine these results, we built up a time dependent photoexcitation code, to model the expected column densities of the Fe II levels as a function of time for an absorber illuminated by a flux such as that of GRB080319B. We obtain smaller values for the distances, namely, ~ 2 and ~ 6 kpc for component I and III, respectively. This discrepancy can be explained by considering the light curve of GRB080319B. The flux of this GRB drops with a steep power law (decay index > 5) in the first 100 s (Racusin et al. 2008b). The steady state approximation assumes a constant flux from the GRB, with this constant being the total fluence radiated up to the moment of the absorption line observation, divided by this time range itself. Thus, this constant is $\sim 10^2$ times higher than the real flux experienced by the absorber at the moment of the first UVES observation. In this scenario, the steady state model will then predict a larger distance in order to account for the higher fluxes at later times.

To assure self-consistency, we need to make sure that, at the smallest distance of 2 kpc as derived for component I, Fe II is not photoionized away by the strong UV radiation of the burst. We showed that there is a wide range of medium densities for which an Fe II absorber at a distance of 2 kpc is not photoionized away by the

radiation from the burst ($10^3 \div 10^{-2}$ cm^{-3}).On the other hand, at densities below ~ 1 cm^{-3}, Mg I is substantially destroyed. Interestingly, component I is the only one for which Mg I is below the detection limit.

Taken at face value, these distances are rather large for a typical galaxy at z$\sim$ 1 (e.g. Sargent et al. 2007) and could imply that the 0.937 system is in the outskirts of the GRB host galaxy or in a nearby clump along the line of sight. Interestingly, HST imaging of the field shows diffuse emission elongated south of the afterglow. In particular, two faint clumps of emissions are located at 1.5″ and 3″ from the afterglow (Tanvir et al. 2008). At z=0.937 these correspond to projected distances of 12 and 24kpc, and may suggest the presence of a complex structure of clumps around the GRB host galaxy. If this is the case, the absorbers may well belong to one of these clumps.

We acknowledge support from ASI/INAF contracts ASI/I/R/039/04 and ASI/I/R/023/05/0. SDV is supported by SFI.

REFERENCES

Ballester, P., Modigliani, A., Boitquin, O. et al. 2000, ESO Messenger, 101, 31
Bloom, J.S., Perley, D.,A., Li, W. et al. 2008, ApJ submintted, astro-ph/0803.3215
Covino, S. et al., 2008a, GCN 7431
Covino, S. et al., 2008b, GCN 7446
Cwiok, M. et al. 2008, GCN 7439
Dekker, H., D'Odorico, S., Kaufer, A., Delabre, B., Kotzlowski, H., 2000, SPIE, 4008, 534
D'Elia, V., Fiore, F., Meurs, E.J.A. et al., 2007, 467, 629
D'Odorico, V., Cristiani, S., Romano, D., Granato, G., & Danese, L. 2004, MNRAS, 424, 23
Fontana, A. & Ballester, P. 1995, The ESO Messenger, 80, 37
Karpov et al. 2008, GCN 7452
Lequeux, J. 2005, The interstellar medium (Translation from the French language edition of: Le Milieu Interstellaire, ed. J. Lequeux, EDP Sciences, 2003), Astronomy and astrophysics library (Berlin: Springer)
Perna, R. & Loeb, A. 1998, ApJ, 501, 467
Perna, R. & Lazzati, D. 2002, ApJ, 580, 261
Prochaska, J. X., Chen, H.-W., & Bloom, J. S. 2006, ApJ, 648, 95
Quinet, P., Le Dourneuf, M., & Zeippen, C. J. 1996, A&AS, 120, 361
Racusin, J.L. et al. 2008a GCN 7427
Racusin, J.L. et al. 2008b, Nature, 455, 183
Sargent, M.T., Carollo, C.M., Lilly, S.J. et al. 2007, ApJS, 172, 434
Silva, A.I., & Viegas, S.M. 2002, MNRAS, 329, 135
Tanvir, N.R. et al. 2008, GCN 7569
Vreeswijk, P.M. et al. 2007, A&A, 468, 83
Vreeswijk, P.M. et al. 2008, GCN 7451